Available online at www.sciencedirect.com
SCIENCE DIRECT®
Journal of Sound and Vibration 278 (2004) 207–231
JOURNAL OF SOUND AND VIBRATION
www.elsevier.com/locate/jsvi

Importance of geometric non-linearity and follower pressure load in the dynamic analysis of a gossamer structure

A.K. Jha[a], D.J. Inman[b,*]

[a] NextGen Aeronautics, 2780 Skypark Drive, Suite 400, Torrance, CA 90505, USA
[b] Department of Mechanical Engineering, Center for Intelligent Material Systems and Structures, Virginia Polytechnic Institute and State University, 310 Durham Hall, Blacksburg, VA 24061-0261, USA

Received 30 September 2002; accepted 2 October 2003

Abstract

Vibration analysis of a gossamer or inflated structure poses special problems, usually not encountered in a conventional metallic or composite structure. In an inflated structure, internal pressure is a major source of strength and rigidity. In the past, most of the studies conducted on the vibration analysis of gossamer structures used inaccurate or approximate theories in modelling the internal pressure. The inexactness in these theories arises due to (1) exclusion of the follower pressure loads, and (2) approximations in the geometric non-linearity. Taking cues from the earlier work done in this area and using line-of-curvature co-ordinates, we re-derive the governing equations for vibration analysis of a shell under pressure, and point out the shortcomings of the previous approximate theories. The same governing equations were derived earlier by Budiansky using tensors. Thereafter, a free-vibration analysis of an inflated torus with free boundary condition is performed using the accurate and the approximate shell theories. It can be seen that the natural frequencies and the mode shapes obtained from the approximate theories are significantly different from those obtained from the accurate shell theory. Since the boundary condition of the torus is free, the vibration analysis should yield six zero frequencies corresponding to the six rigid-body modes. It is shown here that while the accurate theory does give six zero frequencies, the approximate theories do not.

1. Introduction

Gossamer structures, also known as inflatables, possess special properties such as lightweight, minimal stowage volume, and high strength-to-mass ratio. These remarkable properties make them suitable for cost-effective large space antennas, which provide high resolutions and large

*Corresponding author. Tel.: +1-540-231-4709; fax: +1-540-231-2903.
E-mail addresses: ajha@nextgenaero.com (A.K. Jha), dinman@vt.edu (D.J. Inman).

0022-460X/$ - see front matter © 2003 Elsevier Ltd. All rights reserved.
doi:10.1016/j.jsv.2003.10.026

frequency bandwidths. Given the very small wall-thickness, a gossamer structure can be modelled as a shell under pressure. A literature survey on this subject suggests that there have been a very few studies on the vibration analysis of inflatables. Moreover, several of these studies suffer from some serious problems in the ways the effects of pressure have been handled. There are two main effects of pressure.

(1) *Prestress effect*: Pressure induces a prestress field in the structure, which changes the load-bearing capability, or the effective stiffness, of the structure. This effect can be modelled by calculating the prestresses (also called the initial stresses) using the static equations, and then incorporating them into the dynamic equations of motion. Coupling of the prestresses and the dynamic equations of motion can be achieved using geometric non-linearity.

(2) *Follower load effect*: Apart from the prestress effects, the internal pressure also produces the so-called follower load, which arises because the pressure tends to act normal to the deflected surface. The stiffness created by this deflection-dependent force also changes the effective stiffness of the structure.

While a correct shell theory was derived in a previous study using tensors [2], it was not properly applied in several studies regarding the vibration analysis of an inflated structure. In this study, we re-derive these equations for a shell under pressure using the line-of-curvature co-ordinates, and point out the shortcomings of the previous approximate theories. The two effects of pressure were correctly modelled in the dynamic analyses of an inflated torus by Liepins [1] who used the shell theory presented by Budiansky [2], and by Leigh et al. [3] who used finite element code MSC/NASTRAN. Other research work in this area used approximate geometric non-linearities, and ignored altogether the follower force while analyzing an inflated structure (e.g. Refs. [4,5]). In the finite element analysis of Lewis [6], we found that while the prestress effect was properly included, the follower load of the pressure was not. In this paper, we show that these anomalies cause considerable differences in the natural frequencies and mode shapes of an inflated torus.

We follow Sanders' shell theory because of its consistency and good accuracy [7]. First, we derive non-linear strain–displacement relations. Thereafter, we present the basics of Sanders' shell theory for a shell without any pressure load. This shell theory is then modified to include the effects of pressure. To this end, we calculate the strain energy due to prestresses, and the work done by the internal pressure. The variations of the additional strain energy and the work are used in deriving Sanders' shell theory for a shell under pressure. After that, we outline the approximate theories as presented before by other researchers. In order to show the effect of these inaccuracies, we compare the natural frequencies and mode shapes of an inflated torus obtained using different shell theories.

2. Non-linear strain–displacement relations

In order to include the prestress effects of the pressure in the dynamics of an inflatable structure, it is important to use a non-linear strain–displacement relation with the prestresses. Using geometric non-linearity with only the prestresses also maintains the proper homogeneity in the order of the equations, and keeps the resulting equations linear. In this section, we derive non-linear strain–displacement relations from three-dimensional elasticity theory. These relations are later used in deriving the expressions for the strain energy density function.

A shell is defined by a reference surface, thickness of the reference surface, and its edges. Let α_1, α_2, and ζ be the curvilinear co-ordinates system associated with a shell element (Fig. 1). The reference surface, which defines the shape of a shell, is described by two Lamé parameters, A_1 and A_2, and two principal radii of curvatures, R_1 and R_2. In order to define a valid surface, these quantities must satisfy the following three differential equations, known as Gauss–Codazzi conditions [8]:

$$\frac{1}{R_2}\frac{\partial A_1}{\partial \alpha_2} = \frac{\partial}{\partial \alpha_2}\left(\frac{A_1}{R_1}\right), \quad \frac{1}{R_1}\frac{\partial A_2}{\partial \alpha_1} = \frac{\partial}{\partial \alpha_1}\left(\frac{A_2}{R_2}\right), \tag{1}$$

$$\frac{\partial}{\partial \alpha_1}\left(\frac{1}{A_1}\frac{\partial A_2}{\partial \alpha_1}\right) + \frac{\partial}{\partial \alpha_2}\left(\frac{1}{A_2}\frac{\partial A_1}{\partial \alpha_2}\right) = -\frac{A_1 A_2}{R_1 R_2}. \tag{2}$$

Let ε_{ij} denote the strains, where $i,j = 1,2,3$. The symmetry of the three-dimensional elastic strains implies that $\varepsilon_{ij} = \varepsilon_{ji}$. The engineering shear strains (γ_{12}, γ_{13} and γ_{23}) are defined as twice of corresponding tensor shear strains (ε_{12}, ε_{13}, and ε_{23}). The strain–displacement relations for any three-dimensional elastic body in an orthogonal co-ordinate system can be given by [9,10]:

$$\varepsilon_{11} = e_{11} + \tfrac{1}{2}(e_{11}^2 + e_{21}^2 + e_{31}^2), \quad \varepsilon_{22} = e_{22} + \tfrac{1}{2}(e_{22}^2 + e_{12}^2 + e_{32}^2), \tag{3}$$

$$\varepsilon_{33} = e_{33} + \tfrac{1}{2}(e_{33}^2 + e_{13}^2 + e_{23}^2), \quad \gamma_{12} = e_{12} + e_{21} + e_{11}e_{12} + e_{22}e_{21} + e_{31}e_{32}, \tag{4}$$

$$\gamma_{13} = e_{13} + e_{31} + e_{11}e_{13} + e_{33}e_{31} + e_{21}e_{23}, \quad \gamma_{23} = e_{23} + e_{32} + e_{22}e_{23} + e_{33}e_{32} + e_{12}e_{13}, \tag{5}$$

where

$$e_{11} = \frac{1}{H_1}\frac{\partial U_1}{\partial \alpha_1} + \frac{U_2}{H_1 H_2}\frac{\partial H_1}{\partial \alpha_2} + \frac{W}{H_1 H_3}\frac{\partial H_1}{\partial \zeta}, \quad e_{22} = \frac{1}{H_2}\frac{\partial U_2}{\partial \alpha_2} + \frac{U_1}{H_1 H_2}\frac{\partial H_2}{\partial \alpha_1} + \frac{W}{H_2 H_3}\frac{\partial H_2}{\partial \zeta}, \tag{6}$$

$$e_{33} = \frac{1}{H_3}\frac{\partial W}{\partial \zeta} + \frac{U_2}{H_2 H_3}\frac{\partial H_3}{\partial \alpha_2} + \frac{U_1}{H_1 H_3}\frac{\partial H_3}{\partial \alpha_1}, \quad e_{21} = \frac{1}{H_1}\frac{\partial U_2}{\partial \alpha_1} - \frac{U_1}{H_1 H_2}\frac{\partial H_1}{\partial \alpha_2}, \tag{7}$$

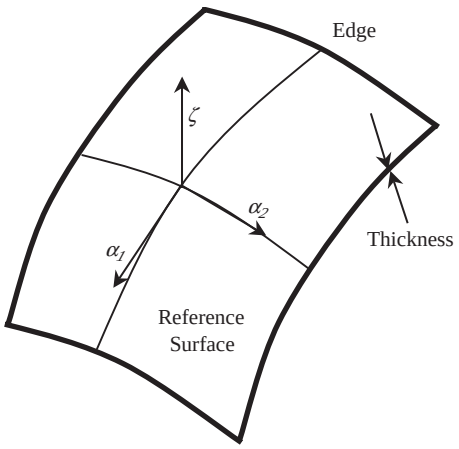

Fig. 1. Shell reference surface with the co-ordinate system.

$$e_{12} = \frac{1}{H_2}\frac{\partial U_1}{\partial \alpha_2} - \frac{U_2}{H_1 H_2}\frac{\partial H_2}{\partial \alpha_1}, \quad e_{13} = \frac{1}{H_3}\frac{\partial U_1}{\partial \zeta} - \frac{W}{H_1 H_3}\frac{\partial H_3}{\partial \alpha_1}, \tag{8}$$

$$e_{31} = \frac{1}{H_1}\frac{\partial W}{\partial \alpha_1} - \frac{U_1}{H_1 H_3}\frac{\partial H_1}{\partial \zeta}, \quad e_{32} = \frac{1}{H_2}\frac{\partial W}{\partial \alpha_2} - \frac{U_2}{H_2 H_3}\frac{\partial H_2}{\partial \zeta}, \quad e_{23} = \frac{1}{H_3}\frac{\partial U_2}{\partial \zeta} - \frac{W}{H_2 H_3}\frac{\partial H_3}{\partial \alpha_2} \tag{9}$$

and where $U_1(\alpha_1, \alpha_2, \zeta, t)$, $U_2(\alpha_1, \alpha_2, \zeta, t)$, and $W(\alpha_1, \alpha_2, \zeta, t)$ are the displacements, and H_1, H_2, and H_3 are the Lamé coefficients of the elastic body along the co-ordinate lines α_1, α_2, and ζ, respectively. For a thin shell, the Lamé coefficients H_1, H_2, and H_3 are given by

$$H_1 = A_1(1 + \zeta/R_1), \quad H_2 = A_2(1 + \zeta/R_2), \quad H_3 = 1. \tag{10}$$

Using the above equation and Gauss–Codazzi conditions, one can evaluate the Eqs. (6)–(9) as

$$e_{11} = \frac{1}{(1 + \zeta/R_1)}\left(\frac{1}{A_1}\frac{\partial U_1}{\partial \alpha_1} + \frac{U_2}{A_1 A_2}\frac{\partial A_1}{\partial \alpha_2} + \frac{W}{R_1}\right), \tag{11}$$

$$e_{22} = \frac{1}{(1 + \zeta/R_2)}\left(\frac{1}{A_2}\frac{\partial U_2}{\partial \alpha_2} + \frac{U_1}{A_1 A_2}\frac{\partial A_2}{\partial \alpha_1} + \frac{W}{R_2}\right), \tag{12}$$

$$e_{21} = \frac{1}{(1 + \zeta/R_1)}\left(\frac{1}{A_1}\frac{\partial U_2}{\partial \alpha_1} - \frac{U_1}{A_1 A_2}\frac{\partial A_1}{\partial \alpha_2}\right), \quad e_{12} = \frac{1}{(1 + \zeta/R_2)}\left(\frac{1}{A_2}\frac{\partial U_1}{\partial \alpha_2} - \frac{U_2}{A_1 A_2}\frac{\partial A_2}{\partial \alpha_1}\right), \tag{13}$$

$$e_{31} = \frac{1}{(1 + \zeta/R_1)}\left(\frac{1}{A_1}\frac{\partial W}{\partial \alpha_1} - \frac{U_1}{R_1}\right), \quad e_{32} = \frac{1}{(1 + \zeta/R_2)}\left(\frac{1}{A_2}\frac{\partial W}{\partial \alpha_2} - \frac{U_2}{R_2}\right), \tag{14}$$

$$e_{33} = \frac{\partial W}{\partial \zeta}, \quad e_{13} = \frac{\partial U_1}{\partial \zeta}, \quad e_{23} = \frac{\partial U_2}{\partial \zeta}. \tag{15}$$

From Love's first approximation, the displacement field can be represented linearly, i.e.,

$$U_1(\alpha_1, \alpha_2, \zeta, t) = u_1(\alpha_1, \alpha_2, t) + \zeta\beta_1(\alpha_1, \alpha_2, t), \tag{16}$$

$$U_2(\alpha_1, \alpha_2, \zeta, t) = u_2(\alpha_1, \alpha_2, t) + \zeta\beta_2(\alpha_1, \alpha_2, t), \tag{17}$$

$$W(\alpha_1, \alpha_2, \zeta, t) = w(\alpha_1, \alpha_2, t), \tag{18}$$

where $u_1(\alpha_1, \alpha_2, t)$, $u_2(\alpha_1, \alpha_2, t)$, and $w(\alpha_1, \alpha_2, t)$ are the mid-surface displacements in α_1, α_2, and ζ directions, respectively. The symbols $\beta_1(\alpha_1, \alpha_2, t)$ and $\beta_2(\alpha_1, \alpha_2, t)$ represent the rotations of tangents of the middle surface oriented along α_1 and α_2 directions, respectively. These rotations can be obtained using Love's first approximation as [8]

$$\beta_1 = \frac{u_1}{R_1} - \frac{1}{A_1}\frac{\partial w}{\partial \alpha_1}, \quad \beta_2 = \frac{u_2}{R_2} - \frac{1}{A_2}\frac{\partial w}{\partial \alpha_2}. \tag{19}$$

Substituting the displacement fields in Eqs. (11)–(15) yields the following relations [10]:

$$e_{11} = \varepsilon_1^0 + \zeta\kappa_1, \quad e_{22} = \varepsilon_2^0 + \zeta\kappa_2, \quad e_{33} = 0, \tag{20}$$

$$e_{21} = \varepsilon_3^0 + \zeta\kappa_3, \quad e_{12} = \varepsilon_4^0 + \zeta\kappa_4, \quad e_{13} = \beta_1, \tag{21}$$

$$e_{31} = \varepsilon_5^0 + \zeta\kappa_5, \quad e_{32} = \varepsilon_6^0 + \zeta\kappa_6, \quad e_{23} = \beta_2, \tag{22}$$

where

$$\varepsilon_1^0 = \frac{1}{(1+\zeta/R_1)}\left(\frac{1}{A_1}\frac{\partial u_1}{\partial \alpha_1} + \frac{u_2}{A_1A_2}\frac{\partial A_1}{\partial \alpha_2} + \frac{w}{R_1}\right), \quad \kappa_1 = \frac{1}{(1+\zeta/R_1)}\left(\frac{1}{A_1}\frac{\partial \beta_1}{\partial \alpha_1} + \frac{\beta_2}{A_1A_2}\frac{\partial A_1}{\partial \alpha_2}\right), \tag{23}$$

$$\varepsilon_2^0 = \frac{1}{(1+\zeta/R_2)}\left(\frac{1}{A_2}\frac{\partial u_2}{\partial \alpha_2} + \frac{u_1}{A_1A_2}\frac{\partial A_2}{\partial \alpha_1} + \frac{w}{R_2}\right), \quad \kappa_2 = \frac{1}{(1+\zeta/R_2)}\left(\frac{1}{A_2}\frac{\partial \beta_2}{\partial \alpha_2} + \frac{\beta_1}{A_1A_2}\frac{\partial A_2}{\partial \alpha_1}\right), \tag{24}$$

$$\varepsilon_3^0 = \frac{1}{(1+\zeta/R_1)}\left(\frac{1}{A_1}\frac{\partial u_2}{\partial \alpha_1} - \frac{u_1}{A_1A_2}\frac{\partial A_1}{\partial \alpha_2}\right), \quad \kappa_3 = \frac{1}{(1+\zeta/R_1)}\left(\frac{1}{A_1}\frac{\partial \beta_2}{\partial \alpha_1} - \frac{\beta_1}{A_1A_2}\frac{\partial A_1}{\partial \alpha_2}\right), \tag{25}$$

$$\varepsilon_4^0 = \frac{1}{(1+\zeta/R_2)}\left(\frac{1}{A_2}\frac{\partial u_1}{\partial \alpha_2} - \frac{u_2}{A_1A_2}\frac{\partial A_2}{\partial \alpha_1}\right), \quad \kappa_4 = \frac{1}{(1+\zeta/R_2)}\left(\frac{1}{A_2}\frac{\partial \beta_1}{\partial \alpha_2} - \frac{\beta_2}{A_1A_2}\frac{\partial A_2}{\partial \alpha_1}\right), \tag{26}$$

$$\varepsilon_5^0 = -\frac{\beta_1}{(1+\zeta/R_1)}, \quad \kappa_5 = -\frac{\beta_1}{(1+\zeta/R_1)R_1}, \quad \varepsilon_6^0 = -\frac{\beta_2}{(1+\zeta/R_2)}, \quad \kappa_6 = -\frac{\beta_2}{(1+\zeta/R_2)R_2}. \tag{27}$$

Now we substitute Eqs. (20)–(22) in Eqs. (3)–(5), and neglect the terms having ζ^2. The remaining part can be separated into two groups based upon dependency on ζ. The group of terms that does not contain ζ represents the changes in lengths of the shell element. The other group represents the changes in the curvatures and the torsion of the reference surface. The following equations summarize the results:

$$\varepsilon_{11} = \varepsilon_1^t + \zeta\kappa_1^t, \quad \varepsilon_{22} = \varepsilon_2^t + \zeta\kappa_2^t, \quad \gamma_{12} = \gamma_{12}^t + \zeta\kappa_{12}^t, \tag{28}$$

where

$$\varepsilon_1^t = \varepsilon_1^0 + \tfrac{1}{2}[\varepsilon_1^{02} + \varepsilon_3^{02} + \varepsilon_5^{02}], \quad \varepsilon_2^t = \varepsilon_2^0 + \tfrac{1}{2}[\varepsilon_2^{02} + \varepsilon_4^{02} + \varepsilon_6^{02}], \tag{29}$$

$$\gamma_{12}^t = \varepsilon_3^0 + \varepsilon_4^0 + \varepsilon_1^0\varepsilon_4^0 + \varepsilon_2^0\varepsilon_3^0 + \varepsilon_5^0\varepsilon_6^0, \quad \kappa_1^t = \kappa_1 + \varepsilon_1^0\kappa_1 + \varepsilon_3^0\kappa_3 + \varepsilon_5^0\kappa_5, \tag{30}$$

$$\kappa_2^t = \kappa_2 + \varepsilon_2^0\kappa_2 + \varepsilon_4^0\kappa_4 + \varepsilon_6^0\kappa_6, \tag{31}$$

$$\kappa_{12}^t = \kappa_3 + \kappa_4 + \kappa_1\varepsilon_4^0 + \varepsilon_1^0\kappa_4 + \kappa_2\varepsilon_3^0 + \varepsilon_2^0\kappa_3 + \kappa_5\varepsilon_6^0 + \varepsilon_5^0\kappa_6. \tag{32}$$

The non-linear terms in the strains ε_{33}, γ_{13}, and γ_{23} are neglected, as they are very small (zero from Love's first approximation). The superscript t in the above equation denotes the total quantity, i.e., summation of both linear and non-linear terms. Since the wall thickness of an inflatable structure is usually very small (a few μm), the prestresses are assumed to be of membrane-type, i.e., uniform throughout the thickness. Therefore, it is sufficient to retain only linear terms in the expressions of changes in curvature and torsion. This implies

$$\kappa_1^t = \kappa_1, \quad \kappa_2^t = \kappa_2, \quad \kappa_{12}^t = \kappa_3 + \kappa_4. \tag{33}$$

In order to satisfy the "sixth equilibrium equation" and the zero strains in small rigid body motions, Sanders [7] defined a new quantity β_n that represents the rotation about the normal to the reference surface, given by

$$\beta_n = \frac{1}{2A_1A_2}\left[\frac{\partial(A_2u_2)}{\partial \alpha_1} - \frac{\partial(A_1u_1)}{\partial \alpha_2}\right]. \tag{34}$$

Using the rotation β_n, a few new strain quantities are defined as

$$\varepsilon_3^s = \varepsilon_3^0 - \frac{\beta_n}{1+\zeta/R_1}, \quad \varepsilon_4^s = \varepsilon_4^0 + \frac{\beta_n}{1+\zeta/R_2}, \tag{35}$$

$$\kappa_3^s = \kappa_3 - \frac{\beta_n/R_1}{1+\zeta/R_1}, \quad \kappa_4^s = \kappa_4 + \frac{\beta_n/R_2}{1+\zeta/R_2}. \tag{36}$$

Expanding the above quantities, and neglecting ζ/R_1 and ζ/R_2 with respect to 1, we get [7]

$$\varepsilon_3^s = \varepsilon_4^s = \frac{1}{2}\left(\frac{1}{A_1}\frac{\partial u_2}{\partial \alpha_1} + \frac{1}{A_2}\frac{\partial u_1}{\partial \alpha_2} - \frac{u_1}{A_1 A_2}\frac{\partial A_1}{\partial \alpha_2} - \frac{u_2}{A_1 A_2}\frac{\partial A_2}{\partial \alpha_1}\right), \tag{37}$$

$$\kappa_3^s - \kappa_4^s = \left(\frac{1}{R_2} - \frac{1}{R_1}\right)\varepsilon_3^s. \tag{38}$$

Using the new definition of strains and again neglecting ζ/R_1 and ζ/R_2 in comparison with 1, we get the in-plane strains as

$$\varepsilon_1^t = \varepsilon_1^0 + \tfrac{1}{2}[\varepsilon_1^{02} + \varepsilon_3^{s2} + 2\varepsilon_3^s\beta_n + \beta_1^2 + \beta_n^2], \tag{39}$$

$$\varepsilon_2^t = \varepsilon_2^0 + \tfrac{1}{2}[\varepsilon_2^{02} + \varepsilon_3^{s2} - 2\varepsilon_3^s\beta_n + \beta_2^2 + \beta_n^2], \tag{40}$$

$$\gamma_{12}^t = \varepsilon_3^0 + \varepsilon_4^0 + \varepsilon_3^s(\varepsilon_1^0 + \varepsilon_2^0) - \beta_n(\varepsilon_1^0 - \varepsilon_2^0) + \beta_1\beta_2. \tag{41}$$

We use the above strain–displacement relations in order to obtain the strain energy density function for a shell under prestresses.

3. Governing equations for a shell without pressure

In this section, we present Sanders' shell theory [7]. In the next section, we derive the necessary modifications in this theory due to the internal pressure. Let N_{11}, N_{22}, N_{12}, N_{21} be the in-plane stress resultants (Fig. 2) and M_{11}, M_{22}, M_{12}, M_{21} be the bending and twisting moment resultants (Fig. 3). The surface traction forces per unit area along the co-ordinates α_1, α_2, and ζ are denoted by q_1, q_2, and q_3, respectively. The transverse shear stress resultants are replaced by the equivalent expressions in the equilibrium equations. The modified membrane shear stress resultant ($\tilde{N}_{12}$), modified twisting moment resultants ($\tilde{M}_{12}$), and the modified twisting strain ($\tilde{\kappa}_{12}$) are defined as [7]

$$\tilde{N}_{12} = \tfrac{1}{2}(N_{12} + N_{21}), \quad \tilde{M}_{12} = \tfrac{1}{2}(M_{12} + M_{21}), \quad \tilde{\kappa}_{12} = \tfrac{1}{2}(\kappa_3^s + \kappa_4^s). \tag{42}$$

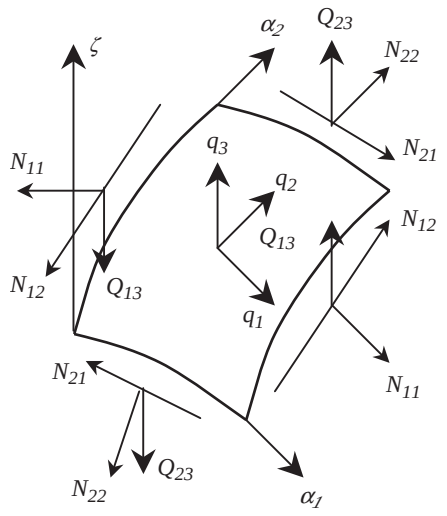

Fig. 2. In-plane stress resultants and external loadings.

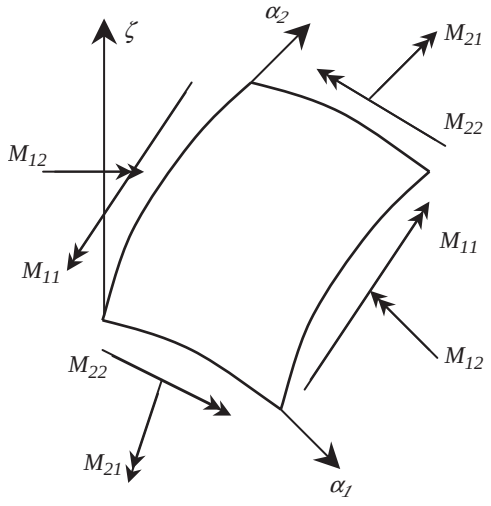

Fig. 3. Bending and twisting moment resultants.

3.1. Equilibrium equations

The equilibrium equations for a shell without any pressure load are given by the following three equations [7]:

$$\frac{\partial(N_{11}A_2)}{\partial\alpha_1}+\frac{\partial(\tilde{N}_{12}A_1)}{\partial\alpha_2}+\tilde{N}_{12}\frac{\partial A_1}{\partial\alpha_2}-N_{22}\frac{\partial A_2}{\partial\alpha_1}+\frac{1}{R_1}\left[\frac{\partial(M_{11}A_2)}{\partial\alpha_1}+\frac{\partial(\tilde{M}_{12}A_1)}{\partial\alpha_2}\right.$$
$$\left.+\tilde{M}_{12}\frac{\partial A_1}{\partial\alpha_2}-M_{22}\frac{\partial A_2}{\partial\alpha_1}\right]+\frac{A_1}{2}\frac{\partial}{\partial\alpha_2}\left[\tilde{M}_{12}\left(\frac{1}{R_1}-\frac{1}{R_2}\right)\right]+A_1A_2(q_1-\rho h\ddot{u}_1)=0, \quad (43)$$

$$\frac{\partial(N_{22}A_1)}{\partial\alpha_2}+\frac{\partial(\tilde{N}_{12}A_2)}{\partial\alpha_1}+\tilde{N}_{12}\frac{\partial A_2}{\partial\alpha_1}-N_{11}\frac{\partial A_1}{\partial\alpha_2}+\frac{1}{R_2}\left[\frac{\partial(M_{22}A_1)}{\partial\alpha_2}+\frac{\partial(\tilde{M}_{12}A_2)}{\partial\alpha_1}+\tilde{M}_{12}\frac{\partial A_2}{\partial\alpha_1}-M_{11}\frac{\partial A_1}{\partial\alpha_2}\right]+\frac{A_2}{2}\frac{\partial}{\partial\alpha_1}\left[\tilde{M}_{12}\left(\frac{1}{R_2}-\frac{1}{R_1}\right)\right]+A_1A_2(q_2-\rho h\ddot{u}_2)=0, \tag{44}$$

$$\frac{\partial}{\partial\alpha_1}\left[\frac{1}{A_1}\left(\frac{\partial(M_{11}A_2)}{\partial\alpha_1}+\frac{\partial(\tilde{M}_{12}A_1)}{\partial\alpha_2}+\tilde{M}_{12}\frac{\partial A_1}{\partial\alpha_2}-M_{22}\frac{\partial A_2}{\partial\alpha_1}\right)\right]+\frac{\partial}{\partial\alpha_2}\left[\frac{1}{A_2}\left(\frac{\partial(M_{22}A_1)}{\partial\alpha_2}+\frac{\partial(\tilde{M}_{12}A_2)}{\partial\alpha_1}+\tilde{M}_{12}\frac{\partial A_2}{\partial\alpha_1}-M_{11}\frac{\partial A_1}{\partial\alpha_2}\right)\right]-A_1A_2\left(\frac{N_{11}}{R_1}+\frac{N_{22}}{R_2}\right)+A_1A_2(q_3-\rho h\ddot{w})=0, \tag{45}$$

where ρ is the density, and h is the wall thickness of the shell. In order to solve the above equilibrium equations, it needs to be expressed in terms of the three mid-surface displacements using the constitutive laws and the strain–displacement relations.

3.2. Constitutive law

The material is assumed to be elastic and isotropic. The constitutive laws, which relate the stress and strain measures, are given by the following equations [7]:

$$N_{11}=K(\varepsilon_1^0+v\varepsilon_2^0),\quad N_{22}=K(\varepsilon_2^0+v\varepsilon_1^0),\quad \tilde{N}_{12}=\frac{K(1-v)}{2}(\varepsilon_3^0+\varepsilon_4^0), \tag{46}$$

$$M_{11}=D(\kappa_1+v\kappa_2),\quad M_{22}=D(\kappa_2+v\kappa_1),\quad \tilde{M}_{12}=D(1-v)\tilde{\kappa}_{12}, \tag{47}$$

where v is the Poisson ratio, K is the membrane stiffness, and D is the bending stiffness. The constants K and D can be written in terms of the Young's modulus (E), the Poisson ratio (v), and thickness (h) of the shell as

$$K=\frac{Eh}{1-v^2},\quad D=\frac{Eh^3}{12(1-v^2)}. \tag{48}$$

We assume that the structural properties of the shell are uniform throughout.

3.3. Boundary conditions

The four boundary conditions at the edge with constant α_1 are as follows [7]:

$$N_{11}=\bar{N}_{11}\quad \text{or } u_1=\bar{u}_1, \tag{49}$$

$$\tilde{N}_{12}+\left(\frac{3}{2R_2}-\frac{1}{2R_1}\right)\tilde{M}_{12}=\bar{N}_{12}+\frac{\bar{M}_{12}}{R_2}\quad \text{or } u_2=\bar{u}_2, \tag{50}$$

$$Q_{13}+\frac{1}{A_2}\frac{\partial\tilde{M}_{12}}{\partial\alpha_2}=\bar{Q}_{13}+\frac{1}{A_2}\frac{\partial\bar{M}_{12}}{\partial\alpha_2}\quad \text{or } w=\bar{w}, \tag{51}$$

$$M_{11}=\bar{M}_{11}\quad \text{or } \beta_1=\bar{\beta}_1. \tag{52}$$

where the quantities with over bar are specified ones. Expression for the boundary conditions at the edge of constant α_2 can be obtained by interchanging 1 and 2 in the above equations.

4. Governing equations for a shell subjected to pressure

Since we assumed the initial stresses to be of membrane type, the prestresses σ^r_{33}, σ^r_{32}, σ^r_{32}, σ^r_{31}, and σ^r_{13}, related to the transverse direction, are assumed negligible. The material is assumed to follow Hooke's Law. Since prestresses σ^r_{ij} are constant in time, and the vibratory stresses σ_{ij} are proportional to ε_{ij}, the strain energy density function can be given by (Fig. 4, Ref. [11])

$$P = \tfrac{1}{2}(\sigma_{11}\varepsilon_{11} + \sigma_{22}\varepsilon_{22} + \sigma_{33}\varepsilon_{33} + \sigma_{23}\varepsilon_{23} + \sigma_{32}\varepsilon_{32} + \sigma_{31}\varepsilon_{31} + \sigma_{13}\varepsilon_{13} + \sigma_{12}\varepsilon_{12} + \sigma_{21}\varepsilon_{21}) + (\sigma^r_{11}\varepsilon_{11} + \sigma^r_{12}\varepsilon_{12} + \sigma^r_{21}\varepsilon_{21} + \sigma^r_{22}\varepsilon_{22}). \tag{53}$$

The terms in the second bracket are the additional terms due to the prestresses. According to Love's first approximation, ε_{33} and σ_{33} are negligibly small, which leads to dropping the terms corresponding to ε_{33} in Eq. (53). Though from Love's first approximation $\delta\gamma_{23}$ and $\delta\gamma_{13}$ are also zero, they are not dropped from the strain energy expression in order keep the non-zero transverse shear stresses (σ_{13}, σ_{23}) in the governing equations. Now, using symmetry of stress and strain tensors, and the definitions of the engineering strains, one can write the above equation as

$$P = \tfrac{1}{2}(\sigma_{11}\varepsilon_{11} + \sigma_{22}\varepsilon_{22} + \sigma_{23}\gamma_{23} + \sigma_{13}\gamma_{13} + \sigma_{12}\gamma_{12}) + (\sigma^r_{11}\varepsilon_{11} + \sigma^r_{12}\gamma_{12} + \sigma^r_{22}\varepsilon_{22}). \tag{54}$$

We concentrate only on the terms in the second bracket of the above equation, which are due to the prestresses. This leads to the following expression for the variation of additional strain energy due to the prestresses:

$$\delta\Delta U_E = \int_V (\sigma^r_{11}\delta\varepsilon_{11} + \sigma^r_{22}\delta\varepsilon_{22} + \sigma^r_{12}\delta\gamma_{12})\,\mathrm{d}V. \tag{55}$$

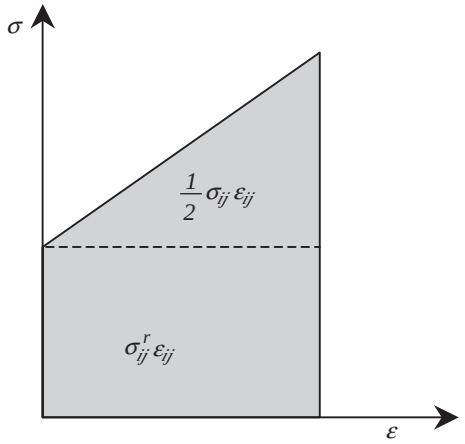

Fig. 4. Initial and vibratory stresses as a function of strain.

The above equation contains the three-dimensional strains, which are next written in terms of two-dimensional strains as

$$\delta\Delta U_E = \int_V \sigma_{11}^r\{(1+\varepsilon_1^0)\delta\varepsilon_1^0 + (\varepsilon_3^s+\beta_n)\delta\varepsilon_3^s + \beta_1\delta\beta_1 + (\varepsilon_3^s+\beta_n)\delta\beta_n + \zeta\delta\kappa_1\} + \sigma_{22}^r\{(1+\varepsilon_2^0)\delta\varepsilon_2^0 + (\varepsilon_3^s-\beta_n)\delta\varepsilon_3^s + \beta_2\delta\beta_2 - (\varepsilon_3^s-\beta_n)\delta\beta_n + \zeta\delta\kappa_2\} + \sigma_{12}^r\{\delta\varepsilon_3^0 + \delta\varepsilon_4^0 + \zeta(\delta\kappa_3+\delta\kappa_4) + (\varepsilon_1^0+\varepsilon_2^0)\delta\varepsilon_3^s + (\varepsilon_3^s-\beta_n)\delta\varepsilon_1^0 + (\varepsilon_3^s+\beta_n)\delta\varepsilon_2^0 - (\varepsilon_1^0-\varepsilon_2^0)\delta\beta_n + \beta_2\delta\beta_1 + \beta_1\delta\beta_2\}\,\mathrm{d}V. \quad (56)$$

Eq. (56) will be used in calculating the variation of the total strain energy, which, in turn, will yield static equations, and couple the prestresses with the dynamic equations.

There are two main ways the work done by pressure can be taken into account. One modelling approach is to consider the pressure force as a dead load. Another approach, which is taken in the present study, is to consider that the pressure force acts normal to the deformed surface during the vibration. Therefore, as the shell vibrates, the direction of the force changes, making it a displacement-dependent force. This effect, called the follower action of pressure load [12], creates the pressure stiffness. For a complete, doubly curved shell, the work done by uniform fluid pressure as the shell deforms is the product of the pressure times the change in the volume enclosed by the shell. Variation of the work done by the pressure p can be written as [2]

$$\delta W_p = \int_{\alpha_2}\int_{\alpha_1} p[\beta_1\delta u_1 + \beta_2\delta u_2 + (\varepsilon_1^0+\varepsilon_2^0)\delta w]A_1A_2\,\mathrm{d}\alpha_1\,\mathrm{d}\alpha_2. \quad (57)$$

Eqs. (56) and (57) can be considered as the addenda to the original expressions of the variations of strain energy and work done used in deriving the Sanders' shell theory [7] for a shell without pressure. Once these quantities are added, the governing equations for a shell subjected to pressure can be obtained using Hamilton's principle. Details of the derivations are omitted here for the sake of brevity. Vibration of a shell under prestress can be analyzed analogously to a spring–mass system under the effect of gravity. In a linear analysis, we can separate the dynamic and static parts. Let N_{11}^r, N_{22}^r, N_{12}^r, and N_{21}^r be the initial in-plane stress resultants, also called the

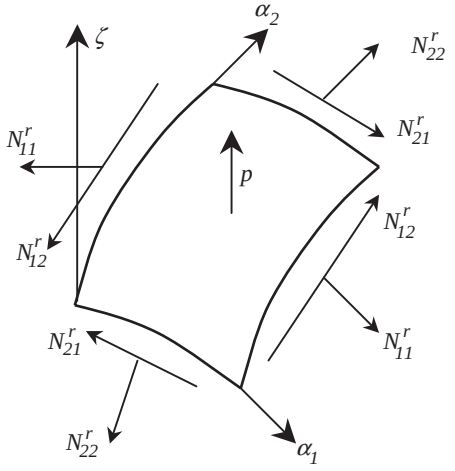

Fig. 5. Initial in-plane stress resultants and the pressure loading.

prestresses (Fig. 5). The modified initial membrane shear stress resultant ($\tilde{N}^r_{12}$) can be defined similar to $\tilde{N}_{12}$ (Eq. (42)). Setting all the quantities related to the vibration of the shell to zero yields the following static equations:

$$\frac{\partial(N^r_{11}A_2)}{\partial\alpha_1}+\frac{\partial(\tilde{N}^r_{12}A_1)}{\partial\alpha_2}+\tilde{N}^r_{12}\frac{\partial A_1}{\partial\alpha_2}-N^r_{22}\frac{\partial A_2}{\partial\alpha_1}=0, \tag{58}$$

$$\frac{\partial(N^r_{22}A_1)}{\partial\alpha_2}+\frac{\partial(\tilde{N}^r_{12}A_2)}{\partial\alpha_1}+\tilde{N}^r_{12}\frac{\partial A_2}{\partial\alpha_1}-N^r_{11}\frac{\partial A_1}{\partial\alpha_2}=0, \tag{59}$$

$$\frac{N^r_{11}}{R_1}+\frac{N^r_{22}}{R_2}=p. \tag{60}$$

The solution of these equations gives initial stresses. Subtracting the static equations from the total equations results in the following three equations of motion:

$$\begin{aligned}
&L_1+\frac{\partial[\{N^r_{11}\varepsilon^0_1+\tilde{N}^r_{12}(\varepsilon^s_3-\beta_n)\}A_2]}{\partial\alpha_1}+\frac{1}{2}\frac{\partial}{\partial\alpha_2}[\{N^r_{11}(\varepsilon^s_3+\beta_n)+N^r_{22}(\varepsilon^s_3-\beta_n)\\
&+\tilde{N}^r_{12}(\varepsilon^0_1+\varepsilon^0_2)\}A_1]+\frac{1}{2}\{N^r_{11}(\varepsilon^s_3+\beta_n)+N^r_{22}(\varepsilon^s_3-\beta_n)+\tilde{N}^r_{12}(\varepsilon^0_1+\varepsilon^0_2)\}\frac{\partial A_1}{\partial\alpha_2}\\
&-\{N^r_{22}\varepsilon^0_2+\tilde{N}^r_{12}(\varepsilon^s_3+\beta_n)\}\frac{\partial A_2}{\partial\alpha_1}-\frac{A_1A_2}{R_1}(N^r_{11}\beta_1+\tilde{N}^r_{12}\beta_2)-\frac{1}{2}\frac{\partial}{\partial\alpha_2}\{N^r_{11}(\varepsilon^s_3+\beta_n)\\
&-N^r_{22}(\varepsilon^s_3-\beta_n)-\tilde{N}^r_{12}(\varepsilon^0_1-\varepsilon^0_2)\}A_1+p\beta_1A_1A_2=0,
\end{aligned} \tag{61}$$

$$\begin{aligned}
&L_2+\frac{\partial[\{N^r_{22}\varepsilon^0_2+\tilde{N}^r_{12}(\varepsilon^s_3+\beta_n)\}A_1]}{\partial\alpha_2}+\frac{1}{2}\frac{\partial}{\partial\alpha_1}[\{N^r_{11}(\varepsilon^s_3+\beta_n)+N^r_{22}(\varepsilon^s_3-\beta_n)\\
&+\tilde{N}^r_{12}(\varepsilon^0_1+\varepsilon^0_2)\}A_2]+\frac{1}{2}\{N^r_{11}(\varepsilon^s_3+\beta_n)+N^r_{22}(\varepsilon^s_3-\beta_n)+\tilde{N}^r_{12}(\varepsilon^0_1+\varepsilon^0_2)\}\frac{\partial A_2}{\partial\alpha_1}\\
&-\{N^r_{11}\varepsilon^0_1+\tilde{N}^r_{12}(\varepsilon^s_3-\beta_n)\}\frac{\partial A_1}{\partial\alpha_2}-\frac{A_1A_2}{R_2}(N^r_{22}\beta_2+\tilde{N}^r_{12}\beta_1)+\frac{1}{2}\frac{\partial}{\partial\alpha_1}\{N^r_{11}(\varepsilon^s_3+\beta_n)\\
&-N^r_{22}(\varepsilon^s_3-\beta_n)-\tilde{N}^r_{12}(\varepsilon^0_1-\varepsilon^0_2)\}A_2+p\beta_2A_1A_2=0,
\end{aligned} \tag{62}$$

$$\begin{aligned}
&L_3-\{N^r_{11}\varepsilon^0_1+\tilde{N}^r_{12}(\varepsilon^s_3-\beta_n)\}\frac{A_1A_2}{R_1}-\{N^r_{22}\varepsilon^0_2+\tilde{N}^r_{12}(\varepsilon^s_3+\beta_n)\}\frac{A_1A_2}{R_2}-\frac{\partial}{\partial\alpha_1}\\
&[A_2(N^r_{11}\beta_1+\tilde{N}^r_{12}\beta_2)]-\frac{\partial}{\partial\alpha_2}[A_1(N^r_{22}\beta_2+\tilde{N}^r_{12}\beta_1)]+p(\varepsilon^0_1+\varepsilon^0_2)A_1A_2=0,
\end{aligned} \tag{63}$$

where L_1, L_2, and L_3 are the left sides of Eqs. (43)–(45), respectively. Another form of the above equations of motion can be obtained by simplifying the above equations using the static equations, Eqs. (58)–(60), and the Gauss–Codazzi conditions, Eqs. (1) and (2).

$$\begin{aligned}
&L_1+A_1A_2N^r_{11}\left(\frac{1}{A_1}\frac{\partial\varepsilon^0_1}{\partial\alpha_1}+\frac{\gamma_{12}}{A_1A_2}\frac{\partial A_1}{\partial\alpha_2}-\frac{\beta_1}{R_1}\right)+2A_1A_2N^r_{12}\left(\frac{1}{A_2}\frac{\partial\varepsilon^0_1}{\partial\alpha_2}-\frac{\gamma_{12}}{A_1A_2}\frac{\partial A_2}{\partial\alpha_1}\right)\\
&+A_1A_2N^r_{22}\left(\frac{1}{2A_2}\frac{\partial\gamma_{12}}{\partial\alpha_2}+\frac{(\varepsilon^0_1-\varepsilon^0_2)}{A_\phi A_s}\frac{\partial A_2}{\partial\alpha_1}-\frac{1}{A_2}\frac{\partial\beta_n}{\partial\alpha_2}\right)+p\beta_1A_1A_2=0,
\end{aligned} \tag{64}$$

$$L_2 + A_1A_2N_{22}^r\left(\frac{1}{A_2}\frac{\partial\varepsilon_2^0}{\partial\alpha_2} + \frac{\gamma_{12}}{A_1A_2}\frac{\partial A_2}{\partial\alpha_1} - \frac{\beta_2}{R_2}\right) + 2A_1A_2N_{12}^r\left(\frac{1}{A_1}\frac{\partial\varepsilon_2^0}{\partial\alpha_1} - \frac{\gamma_{12}}{A_1A_2}\frac{\partial A_1}{\partial\alpha_2}\right)$$
$$+ A_1A_2N_{11}^r\left(\frac{1}{2A_1}\frac{\partial\gamma_{12}}{\partial\alpha_1} + \frac{(\varepsilon_2^0 - \varepsilon_1^0)}{A_1A_2}\frac{\partial A_1}{\partial\alpha_2} + \frac{1}{A_1}\frac{\partial\beta_n}{\partial\alpha_1}\right) + p\beta_2A_1A_2 = 0, \tag{65}$$

$$L_3 - A_1A_2N_{11}^r\left(\frac{\varepsilon_1^0}{R_1} + \frac{1}{A_1}\frac{\partial\beta_1}{\partial\alpha_1} + \frac{\beta_2}{A_1A_2}\frac{\partial A_1}{\partial\alpha_2}\right) - A_1A_2N_{12}^r\left[\frac{1}{A_2}\frac{\partial\beta_1}{\partial\alpha_2} + \frac{1}{A_1}\frac{\partial\beta_2}{\partial\alpha_1}\right.$$
$$\left. - \frac{\beta_1}{A_1A_2}\frac{\partial A_1}{\partial\alpha_2} - \frac{\beta_2}{A_1A_2}\frac{\partial A_2}{\partial\alpha_1} - \left(\frac{1}{R_1} - \frac{1}{R_2}\right)\beta_n + \left(\frac{1}{R_1} + \frac{1}{R_2}\right)\frac{\gamma_{12}}{2}\right] - A_1A_2N_{22}^r$$
$$\times\left(\frac{\varepsilon_2^0}{R_2} + \frac{1}{A_2}\frac{\partial\beta_2}{\partial\alpha_2} + \frac{\beta_1}{A_1A_2}\frac{\partial A_2}{\partial\alpha_1}\right) + A_1A_2p(\varepsilon_1^0 + \varepsilon_2^0) = 0. \tag{66}$$

The above forms of the equations of motion do not contain the derivatives of the prestresses, and were derived previously by Budiansky [2] using tensors. These equations can be solved in conjunction with the boundary conditions presented below to obtain vibratory stresses and the deflections from the equilibrium state. The four boundary conditions at the edge with constant α_1 are as follows:

$$N_{11} + N_{11}^r\varepsilon_{11} + \tilde{N}_{12}^r\left(\frac{\gamma_{12}}{2} - \beta_n\right) = \bar{N}_{11} \quad \text{or } u_1 = \bar{u}_1, \tag{67}$$

$$\tilde{N}_{12} + \left(\frac{3}{2R_2} - \frac{1}{2R_1}\right)\tilde{M}_{12} + \tilde{N}_{12}^r\varepsilon_{22} + N_{11}^r\left(\frac{\gamma_{12}}{2} + \beta_n\right) = \bar{N}_{12} + \frac{\bar{M}_{12}}{R_2} \quad \text{or } u_2 = \bar{u}_2, \tag{68}$$

$$Q_{13} + \frac{1}{A_2}\frac{\partial\tilde{M}_{12}}{\partial\alpha_2} = \bar{Q}_{13} + \frac{1}{A_2}\frac{\partial\bar{M}_{12}}{\partial\alpha_2} \quad \text{or } w = \bar{w}, \tag{69}$$

$$M_{11} = \bar{M}_{11} \quad \text{or } \beta_1 = \bar{\beta}_1, \tag{70}$$

where the quantities with over bar are specified ones. The boundary conditions at the edge with constant α_2 can be obtained by interchanging the suffixes 1 and 2 in the above equations.

5. Approximate shell theories

First, we present approximate geometric non-linearities, which can be used in deriving different theories following the approach suggested in Section 4. For the sake of brevity, the final equations will not be derived in this paper. We start with Sanders' non-linear shell theory [13], which assumes small strains and moderately small rotations. This implies that the linear in-plane membrane strains (ε_1^0, ε_2^0, ε_3^0, and ε_4^0) are much smaller than the rotations (β_1, β_2, and β_n) in Eqs. (39)–(41), and yields the following strain–displacement relations [13]:

$$\varepsilon_1^s = \varepsilon_1^0 + \tfrac{1}{2}[(\beta_n)^2 + (\beta_1)^2], \tag{71}$$

$$\varepsilon_2^s = \varepsilon_2^0 + \tfrac{1}{2}[(\beta_n)^2 + (\beta_2)^2], \tag{72}$$

$$\gamma_{12}^{s} = \varepsilon_3^0 + \varepsilon_4^0 + \beta_1\beta_2. \tag{73}$$

In the above equations, the superscript s denotes the strains corresponding to Sanders' non-linear shell theory. Using the above definitions, one can derive the shell theory and boundary conditions for a shell under pressure corresponding to Sanders' non-linear shell theory. If the terms containing β_n are dropped in the above equations, we get geometric non-linearity, which was used by Plaut et al. [5]:

$$\varepsilon_1^{p} = \varepsilon_1^0 + \tfrac{1}{2}(\beta_1)^2, \tag{74}$$

$$\varepsilon_2^{p} = \varepsilon_2^0 + \tfrac{1}{2}(\beta_2)^2, \tag{75}$$

$$\gamma_{12}^{p} = \varepsilon_3^0 + \varepsilon_4^0 + \beta_1\beta_2. \tag{76}$$

In order to derive the non-linear theory for a shell under prestresses given by Soedel [11], all the squared terms involving u_1 and u_2 are ignored when compared to w in the above equations. This gives

$$\varepsilon_1^{d} = \frac{1}{A_1}\frac{\partial u_1}{\partial \alpha_1} + \frac{u_2}{A_1A_2}\frac{\partial A_1}{\partial \alpha_2} + \frac{w}{R_1} + \frac{1}{2A_1^2}\left(\frac{\partial w}{\partial \alpha_1}\right)^2, \tag{77}$$

$$\varepsilon_2^{d} = \frac{1}{A_2}\frac{\partial u_2}{\partial \alpha_2} + \frac{u_1}{A_1A_2}\frac{\partial A_2}{\partial \alpha_1} + \frac{w}{R_2} + \frac{1}{2A_1^2}\left(\frac{\partial w}{\partial \alpha_1}\right)^2, \tag{78}$$

$$\gamma_{12}^{d} = \frac{1}{A_1}\frac{\partial u_2}{\partial \alpha_1} - \frac{u_1}{A_1A_2}\frac{\partial A_1}{\partial \alpha_2} + \frac{1}{A_2}\frac{\partial u_1}{\partial \alpha_2} - \frac{u_2}{A_1A_2}\frac{\partial A_2}{\partial \alpha_1} + \frac{1}{A_1A_2}\frac{\partial w}{\partial \alpha_1}\frac{\partial w}{\partial \alpha_2}. \tag{79}$$

The above definitions are known as Donnell's non-linear shell theory [14]. The bending and the torsion strains for this case are given in Eq. (33). In deriving the equations corresponding to those by Soedel [11], one also needs to ignore the changes in definitions due to Sanders [7] as presented in Eq. (42). Note that the original Sanders non-linear shell theory [13] was not derived for a shell under pressure. Hence, to derive his original equations, one will have to replace all the prestresses with the vibratory stresses, and will have to ignore the follower pressure load. Plaut et al. [5] analyzed an inflated toroidal structure under various types of snow loads, and Saigal et al. [4] used an approximated version of the equations of Soedel [11] to analyze a tire under internal pressure. Plaut et al. [5] and Soedel [11] considered only the prestresses, and to derive the equations presented by these researchers, one will have to ignore the follower pressure load. In the next section, we present free-vibration analyses of an inflated torus using different shell theories.

6. Numerical results

In this section, we perform a free-vibration analysis of a complete (no free edges) inflated toroidal shell of circular cross-section and free boundary condition using an accurate shell theory (Eqs. (64)–(66)) and compare the results with those obtained using approximate shell theories.

6.1. Free-vibration analysis using an accurate shell theory

The middle surface of the toroidal shell is generated by the revolution of a circle of radius r, with center at a distance $R(=1/\kappa)$ from the axis of revolution (Fig. 6). The Lamé parameters A_1 and A_2 and the principal radii of curvatures R_1 and R_2 are as follows [5]:

$$A_1 = r, \quad A_2 = 1 + r\kappa \cos \alpha_1, \tag{80}$$

$$R_1 = r, \quad R_2 = r + \frac{1}{\kappa \cos \alpha_1}. \tag{81}$$

The above parameters are substituted in the static and dynamic equations so as to specialize the equations for a toroidal shell subjected to pressure. In 1965, Liepins studied the free-vibration analysis of an inflated torus. He solved the governing equations using a finite difference method, and obtained the frequencies and mode shapes by a trial and error method in the Holzer fashion. In the present work, we are using Galerkin's method and mode shapes are given by Fourier series along the tube of the torus and single term sine and cosine function along the circumference [15]. Inflatable structures are often made of Kapton®, and hence its properties will be used in this analysis. The internal pressure has been taken to be 0.5 psi, as it is the desired internal pressure for inflatable satellites [16]. Table 1 shows the data for the geometry and material of the inflatable torus.

Since the boundary conditions of the inflated torus are taken to be free, the free-vibration analysis should also show rigid-body motions. Rigid-body motions in a flexible structure are caused by those deflections where the relative positions of any two particles of the structure do not change with time. A non-trivial situation where these types of deflections are possible is when the *whole* structure is under motion without the relative movement of any two points in the structure. For a structure with all boundary conditions free, any such motion can be decomposed into three pure translations along three perpendicular axes and three pure rotations about the same (Fig. 7). Since the relative displacements of two points are always zero, these motions cause no strain, and hence no restoring elastic force in the structure. This leads to a non-oscillating deflection, and

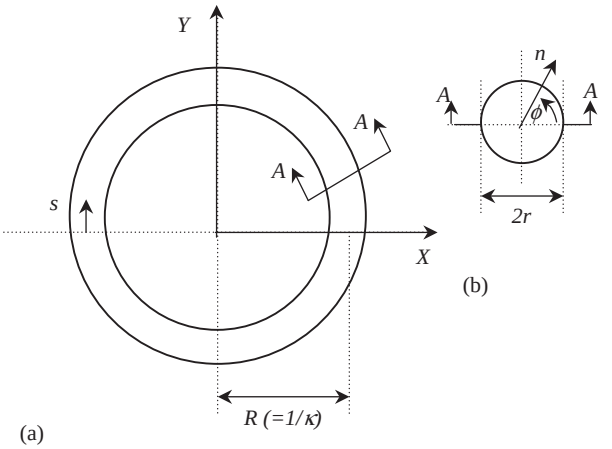

Fig. 6. Geometry of the torus: (a) side view; (b) section A–A.

Table 1
Data for the geometry and material of the torus

Parameter	Values
Elastic modulus (E) (N/m^2)	2.55×10^9
Wall thickness (h) (m)	76.2×10^{-6}
The Poisson ratio (v)	0.34
Density (ρ) (Kg/m^3)	1418
Radius of torus (R) (m)	7.62
Radius of the cross-section (r) (m)	1.22
Internal pressure (p) (N/m^2)	3447.38

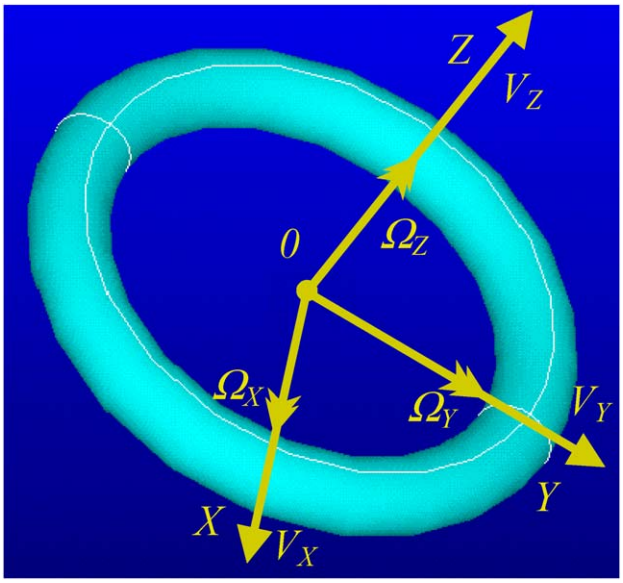

Fig. 7. Directions of displacements and rotations of the rigid-body modes of the inflated torus.

gives rise to zero frequency. Apart from the vibratory strains, forces in a structure could be also caused by other sources, such as gravitational force, initial stresses, pressure, etc. However, there should be no net oscillating force acting on the structure in a rigid body motion. In the case of a torus, the six rigid-body motion can be given by [17]:

(1) Displacement (V_Z) parallel to the axis of symmetry:

$$u_1(\alpha_1, \alpha_2, t) = A\cos(\alpha_1), \quad u_2(\alpha_1, \alpha_2, t) = 0, \quad w(\alpha_1, \alpha_2, t) = A\sin(\alpha_1). \tag{82}$$

(2) Displacements (V_X and V_Y) perpendicular to the axis of symmetry:

$$\begin{aligned} &u_1(\alpha_1, \alpha_2, t) = A\sin(\alpha_1)\cos(\alpha_2/R), \quad u_2(\alpha_1, \alpha_2, t) = A\sin(\alpha_2/R), \\ &w(\alpha_1, \alpha_2, t) = -A\cos(\alpha_1)\cos(\alpha_2/R) \end{aligned} \tag{83}$$

$$u_1(\alpha_1,\alpha_2,t) = A\sin(\alpha_1)\sin(\alpha_2/R), \quad u_2(\alpha_1,\alpha_2,t) = -A\cos(\alpha_2/R),$$
$$w(\alpha_1,\alpha_2,t) = -A\cos(\alpha_1)\sin(\alpha_2/R). \tag{84}$$

(3) Rotation (Ω_Z) about the axis of symmetry:

$$u_1(\alpha_1,\alpha_2,t) = 0, \quad u_2(\alpha_1,\alpha_2,t) = A\{R + r\cos(\alpha_1)\}, \quad w(\alpha_1,\alpha_2,t) = 0. \tag{85}$$

(4) Rotations (Ω_X and Ω_Y) about axes perpendicular to the axis of symmetry:

$$u_1(\alpha_1,\alpha_2,t) = A\{r + R\cos(\alpha_1)\}\cos(\alpha_2/R), \quad u_2(\alpha_1,\alpha_2,t) = Ar\sin(\alpha_1)\sin(\alpha_2/R),$$
$$w(\alpha_1,\alpha_2,t) = AR\sin(\alpha_1)\cos(\alpha_2/R) \tag{86}$$

$$u_1(\alpha_1,\alpha_2,t) = A\{r + R\cos(\alpha_1)\}\sin(\alpha_2/R), \quad u_2(\alpha_1,\alpha_2,t) = -Ar\sin(\alpha_1)\cos(\alpha_2/R),$$
$$w(\alpha_1,\alpha_2,t) = AR\sin(\alpha_1)\sin(\alpha_2/R). \tag{87}$$

The six zero natural frequencies corresponding to the six rigid-body motions were obtained using Eqs. (64)–(66). The non-rigid-body natural frequencies and mode shapes with their projections on one plane are shown in Fig. 8. Vibration modes of an inflated torus can be divided into two main groups: (1) symmetric modes, and (2) antisymmetric modes. These modes are defined according to the deformation of the cross-section of the torus. For example, the cross-section deforms symmetrically about the line passing through $\alpha_1 = 0$ and π in a symmetric mode. Modes 1 and 3 are the out-of-plane bending modes. These modes resemble the bending modes of a free–free beam, and they are produced by the antisymmetric modes. Modes 2 and 5 are symmetric modes. In modes 2 and 5, the torus vibrates by forming elliptical and triangular shapes, respectively. These modes can be termed as the in-plane bending modes. Mode 4 is an axisymmetric mode, where the shape does not change along the torus, and mode 6 is a twisting mode. Modes 4 and 6 are of the antisymmetric type.

6.2. *Effects of the follower pressure load*

In this section, we evaluate the effect of the follower action of pressure. Fig. 9 compares the natural frequencies calculated first using Eqs. (64)–(66), and then using the same equations but without the follower pressure load terms $p\beta_1 A_1 A_2$, $p\beta_2 A_1 A_2$, and $A_1 A_2 p(\varepsilon_1^0 + \varepsilon_2^0)$. It can be seen from Fig. 9 that the difference in the first frequency from the two analysis in around 25%. Similarly, the difference in the second frequency is around 50%. Other frequencies can be also seen in significant differences. The effect of the follower pressure load on the mode order is shown in Table 2. The modes in each case are arranged in the increasing order of corresponding frequencies. A particular entry of the table denotes which mode shape from the correct theory occupies that position. The bold numbers denote the changed positions. For example, in the case of no follower load, the third row entry is 5. It means that if we arrange the mode shapes calculated by discarding the follower load in the increasing order of natural frequency, the third mode will be actually the fifth mode obtained using the correct theory. It can be seen that almost all of the modes are in incorrect sequence. Another effect of excluding the pressure force is that the relative cross-sectional deformation of modes becomes higher (Fig. 10).

Since the boundary condition of the torus is free, the free-vibration analysis should yield six zero frequencies. We found that the exclusion of follower pressure load produces incorrect natural

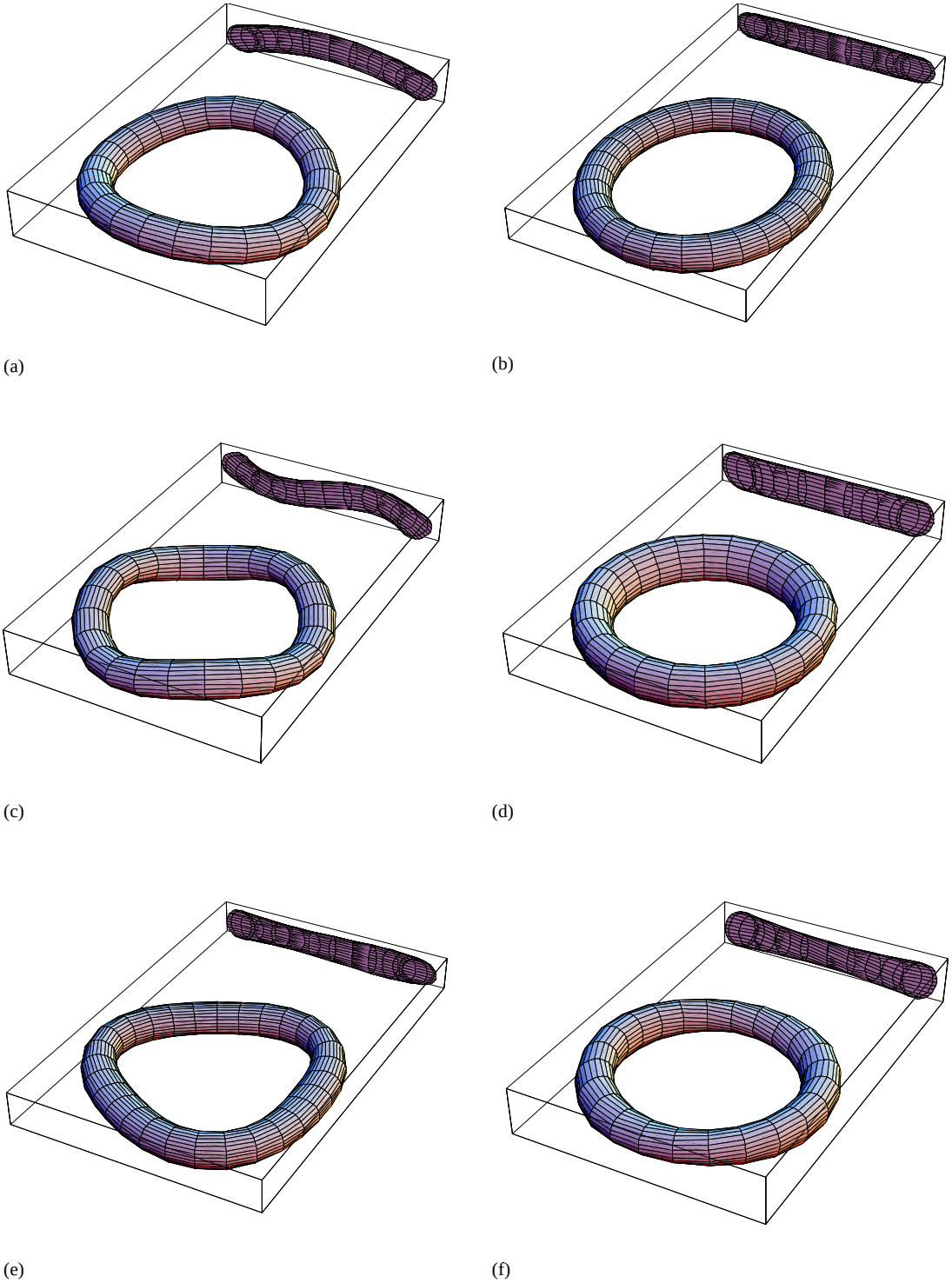

Fig. 8. The first six natural frequencies and mode shapes of the inflated torus: (a) mode 1 (6.90 Hz), first out-of-plane bending mode; (b) mode 2 (7.24 Hz), first in-plane bending mode; (c) mode 3 (17.71 Hz), second out-of-plane bending mode; (d) mode 4 (17.85 Hz), first axisymmetric mode; (e) mode 5 (18.55 Hz), second in-plane bending mode; (f) mode 6 (24.85 Hz), third antisymmetric mode (twisting).

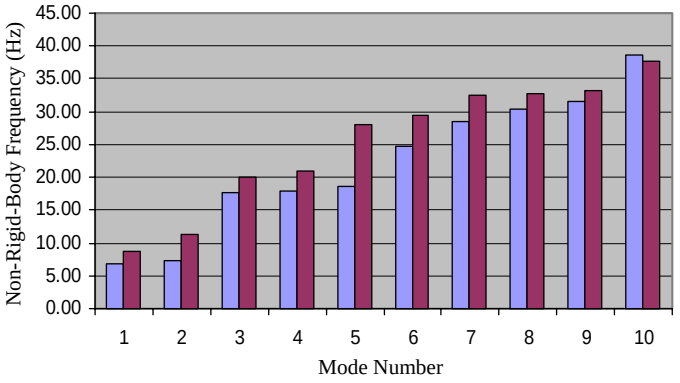

Fig. 9. Comparison of the natural frequencies calculated considering the follower pressure load (first bar) and neglecting the follower pressure load (second bar).

Table 2
Comparison of mode orders with and without considering follower pressure load

Mode number	With follower pressure load	Without follower pressure load
1	1	2
2	2	1
3	3	5
4	4	3
5	5	7
6	6	4
7	7	8
8	8	9
9	9	6
10	10	10

frequencies corresponding to the rigid-body modes of rotation type (modes 4–6 in Table 3). However, the translation-type rigid-body modes do yield zero frequencies.

As mentioned earlier, there should be no net force acting on the structure in a rigid-body motion. A prestressed structure, such as an inflated torus, with all free boundary conditions can remain in equilibrium with a dead pressure load (one which does not change direction) in no-deflection condition. Under pure translations also, the same equilibrium can be maintained because the direction of the pressure load does not change. However, once the structure is in rotation, the dead load *cannot* maintain the equilibrium with the prestresses. It is because as the structure rotates, the directions of the follower force, which always acts normal to the surface, changes. Therefore, one needs to include follower effect in the equations of motion. Otherwise, it produces a net force on the structure, and hence non-zero frequencies. This is why the three translations do not cause non-zero frequencies but the three rotations do. For example, consider the rotation about the axis of symmetry (Eq. (85)). It leads to zero strains but the following

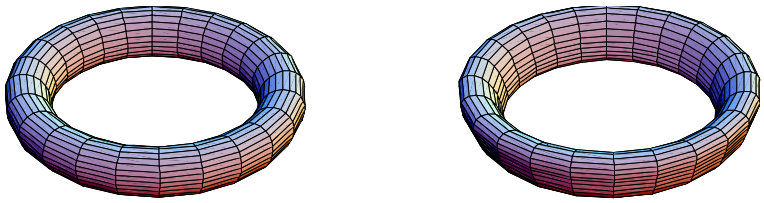

(a) (b)

Fig. 10. Effect of the follower pressure load on the deformation of modes: (a) 17.85 Hz, mode number = 6, with follower force effect; (b) 29.50 Hz, mode number = 6, without follower force effect.

Table 3
Comparison of natural frequencies of rigid-body modes

Rigid-body mode	With follower pressure load	Without follower pressure load
1 (V_Z)	0	0
2 (V_X)	0	0
3 (V_Y)	0	0
4 (Ω_Z)	0	3.99
5 (Ω_X)	0	4.83
6 (Ω_Y)	0	4.83

rotations:

$$\beta_1 = 0, \quad \beta_2 = A\cos(\alpha_1), \quad w(\alpha_1, \alpha_2, t) = -A\sin(\alpha_1). \tag{88}$$

The above rotations yield the following net forces due to prestresses:

$$f_1 = 0, \quad f_2 = -\frac{Apr\cos(\alpha_1)\{R + r\cos(\alpha_1)\}}{R}, \quad f_3 = 0. \tag{89}$$

Therefore, there appears to be a net force in α_2 direction. However, if we included the follower load, the above force is cancelled by the force $Apr\cos(\alpha_1)\{R + r\cos(\alpha_1)\}/R$ generated by the internal pressure. Therefore, the pure rotation about the axis of symmetry, given by Eq. (85), satisfies the equilibrium equations only in the presence of follower pressure load, giving rise to a zero frequency.

The effect of follower pressure load will depend upon the internal pressure, wall thickness, and the elastic modulus of the inflated torus. This effect will be higher for higher internal pressure and smaller wall thickness and lower elastic modulus (and vice versa). Therefore, it is important to know how these parameters as a whole affect the natural frequencies. To this end, the frequencies are plotted against a non-dimensional quantity ζ, called prestress parameter, defined as [1]

$$\zeta = \frac{pr}{Eh}. \tag{90}$$

Fig. 11 shows the effect of the follower pressure load on the first natural frequency (non-rigid-body type). As expected, at very low pressure, the effect of follower pressure load is small and the two results are almost the same. Also, as ζ increases, the natural frequency increases. This is because internal pressure increases the effective stiffness of the structure. Fig. 12 shows that the

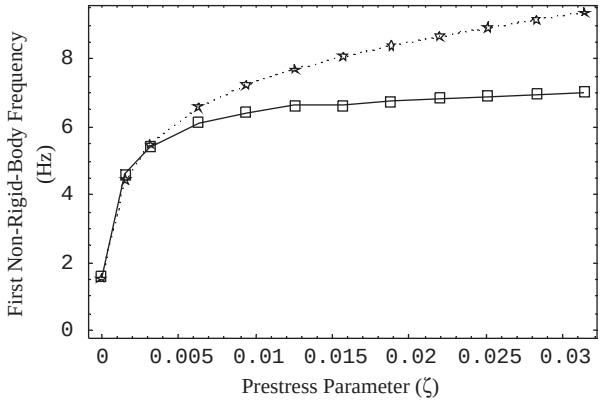

Fig. 11. Effect of prestress parameter on the first non-rigid-body frequency calculated considering the follower pressure load (lower curve) and ignoring the follower pressure load (upper curve).

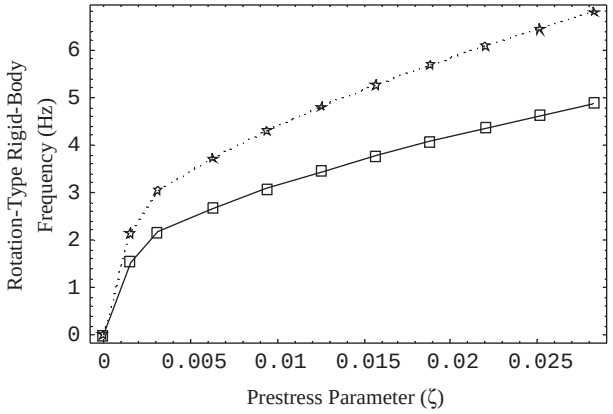

Fig. 12. Effect of prestress parameter on the rigid-body frequencies corresponding to Ω_Z (lower curve), Ω_X and Ω_Y (upper curve) when the follower pressure load is ignored.

rotational-type rigid-body frequencies also increase with the prestress parameter when the follower pressure load is not considered.

6.3. *Effects of approximations in geometric non-linearities*

As seen earlier, consideration of geometric non-linearity is important as it couples the prestresses with the dynamic equations of motion. We consider the following four strain–displacement relations:

(1) Geometric non-linearity (Eqs. (39)–(41)) without any approximations related to the magnitudes of strains and displacements in the in-plane strains.

(2) Sanders' non-linear theory (Eqs. (71)–(73)).

(3) Geometric non-linearities used by Plaut et al. (Eqs. (74)–(76)).

(4) Donnell's non-linear theory (Eqs. (77)–(79)).

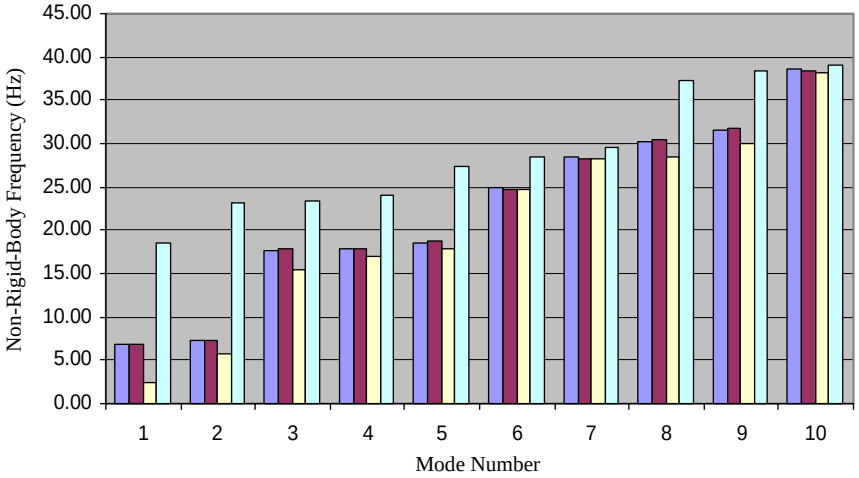

Fig. 13. Comparison of natural frequencies obtained using Cases 1 (first bar), 2 (second bar), 3 (third bar), and 4 (fourth bar).

Table 4
Mode order of the first 10 modes calculated using different theories

Mode number	Case (1)	Case (2)	Case (3)	Case (4)
1	1	1	1	**4**
2	2	2	2	**1**
3	3	**4**	3	**2**
4	4	**3**	**5**	**3**
5	5	5	**4**	**6**
6	6	6	6	**8**
7	7	7	7	**5**
8	8	8	8	**10**
9	9	9	9	**7**
10	10	10	10	**9**

We keep the follower pressure load in all these analyses in order to exclusively point out the effects of approximations in geometric non-linearity. The natural frequencies and modes shapes calculated using the above four cases are compared in Fig. 13. The four bars of a particular mode are arranged in the increasing order of approximation (Case (1) is most accurate and Case (4) is the least). A noticeable point in the figure is that Case (2) gives almost the same result as obtained using Case (1). The results from the other two theories are not so accurate. The first frequency obtained using Case (3) is less than half of the frequency by Case (1). The differences are higher in the lower-order frequencies. On the other hand, the first frequency corresponding to Donnell's non-linearity, Case (4), is more than double of that from Case (1). Other frequencies corresponding to Case (4) are also significantly different, making it almost unusable in the present case.

The visible effects of these approximations on the mode shapes is that the order of modes changes. Table 4 lists the mode orders as given by different theories. We see that the change in

Table 5
Rigid-body frequency calculated using different theories

Rigid-body mode	Frequency (Hz) Case (1)	Frequency (Hz) Case (2)	Frequency (Hz) Case (3)	Frequency (Hz) Case (4)
1 (V_Z)	0	0	1	25.74
2 (V_X)	0	0	2	18.26
3 (V_Y)	0	0	3	18.26
4 (Ω_Z)	0	0	3.50 i	0
5 (Ω_X)	0	0	3.45 i	25.04
6 (Ω_Y)	0	0	3.45 i	25.04

mode order occurs only in two locations in Cases (2) and (3), while there are several changes in Case (4). This suggests that approximation produces incorrect order of mode shapes.

Similar to the case of no follower load, we found that approximations in the geometric non-linearity could lead to non-zero rigid-body frequencies. Case (1) and Case (2) produce the six zero rigid-body frequencies. The theory corresponding to Case (3) gives zero frequencies for the translation-type rigid-body modes and nonzero complex numbers for the rotation-type rigid-body modes. Case (4) produces rigid-body frequencies of the same order as the first non-rigid-body frequency calculated by the same theory. The reason for non-zero rigid-body frequency is again the unbalanced forces (caused this time by the approximation in geometric non-linearity) (Table 5).

From the comparison of rigid-body and non-rigid-body frequencies and mode shapes, one can infer that the rotation of the reference surface about the normal and the in-plane displacements are too important to ignore in the geometric non-linearity for the present case.

Fig. 14 shows how the first and the second natural frequencies calculated using Cases (1), (3), and (4) changes with the prestress parameter (ζ). Case (2) was not included as it always gives frequencies close to those obtained using Case (1). As expected, all three analyses give the same frequencies at $\zeta = 0$, which corresponds to no initial stresses or infinitely stiff torus. However, as ζ grows, the results of Cases (3) and (4) start deviating from the result of Case (1). The same phenomenon is noted regarding other frequencies. From Fig. 14, one can conclude that even for a small prestress parameter, the differences in the results produced by different theories could be significant.

The torus considered in the structure is assumed to be of uniform thickness and material properties. Boundary conditions were also assumed to be completely free. In reality, due to manufacturing limitations, the torus cannot be made perfectly uniform. Often, overlapping membranes are attached using some kind of glue, which add extra mass and stiffness to the structure. Moreover, the present study did not consider the effects of internal and external air. Given the lightweight and the very low stiffness, the behavior of an inflatable structure becomes quite sensitive to these boundary conditions and structural imperfections. It has been shown in the past that the mass of air decreases the natural frequencies and increases the damping of the structure [18,19]. For this reason, Griffith and Main [20], in their experimental study, used a lightweight accelerometer, and took the measurement perpendicular to the gravity field in order to minimize the mass loading effect. They found that with increase in the internal pressure, the

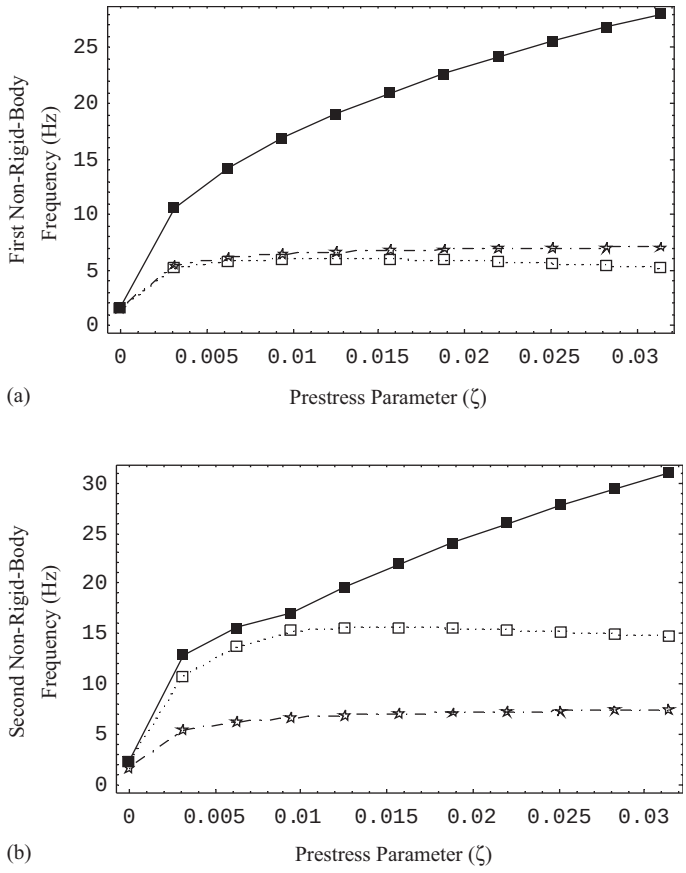

Fig. 14. Effect of prestress parameter on the first two natural frequencies as calculated using different geometric non-linearities: (a) first natural frequency; (b) second natural frequency; ■, Case 1; □, Case 2; ★, Case 3.

natural frequency and structural damping increase, and the viscous damping decreases. Dynamic testing results in vacuum and ambient condition were compared by Slade et al. [21]. They found significant differences in the modal damping and the mass of the air contained by the inflatable structure in the two conditions. Attempts have been also made in the past to model these effects analytically. Leigh and Tinker [22] used MSC/NASTRAN to model the flanges and glues, and found their effects on natural frequencies and mode shapes quite significant. A short discussion on the mass of internal air in an inflated structure can be found in Ref. [23]. However, analytical work in this area is far from complete.

7. Conclusions

The main objective of this paper was to show the effects of approximations in non-linear strain–displacement relations, and exclusion of the follower actions of pressure force on the vibration analysis of an inflated structure. We followed Sanders' shell theory, which was originally given for a shell without pressure load. The necessary modifications for a shell subjected to a pressure load

were derived. The mode shapes and natural frequencies for both rigid-body and non-rigid-body modes were presented. We discussed the effects of (1) follower pressure force and (2) geometric non-linearity, separately. For the first case, we compared the natural frequencies with and without considering the follower force due to pressure. It was observed that the accurate theory gives exactly zero frequencies for the six rigid-body modes, which is consistent with the fact that the torus has free boundary conditions. We found that rotation-type rigid-body frequencies are non-zero when the follower force is not included. The non-rigid-body frequencies were also found be significantly different from the correct ones. For the second case, we considered four different types of geometric non-linearity and compared the natural frequencies and mode shapes. We found that Sanders' non-linear theory performs almost the same as the theory that does not make any assumption regarding the magnitudes of strains and rotation. It was found that the other two approximations lead to non-zero rigid-body frequencies. Also, they differ significantly from the correct results in the non-rigid-body frequencies and mode shapes. It was found that exclusion of rotations in the geometric non-linearity produces more severe effects. From these analyses, it is evident that accuracy in geometric non-linearity as well as the follower action of pressure force is important to consider for acceptable vibration analysis results of an inflated structure.

Acknowledgements

This work was sponsored by the Air Force Office of Scientific Research under Grant number F49620-99-1. The authors gratefully acknowledge this support. The authors are also grateful to Dr. Raymond Plaut of Virginia Polytechnic Institute and State University for helpful discussions.

References

[1] A.A. Liepins, Free vibrations of prestressed toroidal membrane, *American Institute of Aeronautics and Astronautics Journal* 3 (1965) 1924–1933.
[2] B. Budiansky, Notes on nonlinear shell theory, *Journal of Applied Mechanics* 35 (2) (1968) 393–401.
[3] L. Leigh, H. Hamidzadeh, M.L. Tinker, K.N. Slade, Dynamic characterization on an inflatable concentrator for solar thermal propulsion, *Proceedings of the 42nd AIAA/ASME/ASCE/AHS/ASC Structures, Structural Dynamics, and Materials Conference and Exhibit*, Seattle, WA, March 15–19, 2001, pp. 1–7.
[4] S. Saigal, T.Y. Yang, H.W. Kim, W. Soedel, Free vibration of a tire as a toroidal membrane, *Journal of Sound and Vibration* 107 (1986) 71–82.
[5] R.H. Plaut, J.K.S. Goh, M. Kigudde, D.C. Hammerand, Shell analysis of an inflatable arch subjected to snow and wind loading, *International Journal of Solids and Structures* 37 (2000) 4275–4288.
[6] J.A. Lewis, Finite Element Modeling and Active Control of an Inflated Torus Using Piezoelectric Devices, MS Thesis, Mechanical Engineering, Virginia Polytechnic Institute and State University, 2000.
[7] J.L. Sanders, An improved first approximation theory for thin shells, NASA Report, 24 June 1959.
[8] H. Kraus, *Thin Elastic Shells*, Wiley, New York, 1967.
[9] A.S. Saada, *Elasticity: Theory and Applications*, Pergamon Press, New York, 1974.
[10] J.G. Teng, T. Hong, Nonlinear thin shell theories for numerical buckling predictions, *Thin-Walled Structures* 31 (1998) 89–115.
[11] W. Soedel, *Vibrations of Shells and Plates*, Marcel Dekker, New York, 1986.
[12] D.O. Brush, B.O. Almroth, *Buckling of Bars, Plates, and Shells*, McGraw-Hill, New York, 1975.
[13] J.L. Sanders, Nonlinear theories for thin shells, *Quarterly of Applied Mathematics* 21 (1963) 21–36.

[14] L.H. Donnell, Stability of thin-walled tubes under torsion, NACA Report 479, 1934.
[15] A.K. Jha, D.J. Inman, R.H. Plaut, Free vibration analysis of an inflated toroidal shell, *Journal of Vibration and Acoustics* 124 (2002) 387–396.
[16] M.L. Tinker, Passively adaptive inflatable structure for the shooting star experiment, AIAA Paper No. 98-1986, 1998, pp. 2320–2326.
[17] E.E. Kordes, Vibration Analysis of Toroidal Shells of Circular Cross Section, Ph.D. Dissertation, Engineering Mechanics, Virginia Polytechnic Institute and State University, 1960.
[18] J.L. Sewall, R. Miserentino, R.S. Pappa, Vibration studies of a lightweight three-sided membrane suitable for space application, NASA TP 2095, January 1983.
[19] A. Giraudeau, F. Pierron, J.-P. Chambard, Experimental study of air effect on vibrating lightweight structures, *Proceedings of the SEM Annual Conference*, Milwaukee, WI, 10–12 June 2002.
[20] D.T. Griffith, J.A. Main, Experimental modal analysis and damping estimation for an inflated thin-film torus, *Journal of Guidance, Control, and Dynamics* 25 (2002) 609–617.
[21] K.N. Slade, M.L. Tinker, J.O. Lassiter, R. Engberg, Comparison of dynamic characteristics for an inflatable solar concentrator in atmospheric and thermal vacuum conditions, *Proceedings of the 41st AIAA/ASME/ASCE/AHS/ASC Structures, Structural Dynamics, and Material Conference and Exhibit*, Atlanta, GA, Vol. 4, 2000, pp. 64–75.
[22] L.M. Leigh, M.L. Tinker, Dynamic characterization of an inflatable concentrator for solar thermal propulsion, *Journal of Spacecraft and Rockets* 40 (2003) 24–27.
[23] K.B. Smalley, M.L. Tinker, W.S. Taylor, Structural modeling of a five-meter thin-film inflatable antenna/concentrator, *Journal of Spacecraft and Rockets* 40 (2003) 27–29.